Tetraquarks, Σ baryon spectroscopy, and small-interaction scattering from lattice field theory

Daniel James Darvish

Submitted in partial fulfillments of the requirements for the degree of
Doctor of Philosophy
at

Carnegie Mellon University
Department of Physics
Pittsburgh, Pennsylvania
Advisor: Colin J. Morningstar

September, 2020

Abstract

"Young man, in mathematics you don't understand things. You just get used to them." — John von Neumann

Dedication

Lorem ipsum.

Declaration

Lorem ipsum.

Acknowledgements

Lorem ipsum.

Contents

1 Introduction **6**

2 Lattice QCD **7**

3 Building Operators for Finite-Volume Spectroscopy **8**

3.1 Basic Building Blocks 8

3.1.1 Stout Smearing 8

3.1.2 LapH Smearing 9

3.1.3 Displacements 12

3.2 Symmetries on the Lattice 13

3.2.1 Rotations 13

3.2.2 Isospin and Quark Flavor 16

3.2.3 Charge Conjugation and G-Parity 18

3.2.4 Projecting Operators onto Symmetry Sectors 19

3.3 Single-Hadron Operator Construction 19

3.3.1 Baryon Operators 19

3.3.2 Meson Operators 19

3.3.3 Tetraquark Operators 19

3.4 Multi-Hadron Operator Construction 19

4 Monte Carlo Calculation of Correlators **20**

5 Correlator Analysis: Determining the Finite-Volume Spectrum **21**

6 Scattering Resonances in a Two-Scalar Field Theory **22**

7 Investigating the Tetraquark Content of the Light Scalar Mesons κ and $a_0(980)$ **23**

7.1 Operator construction 24

7.2 Lattice Spectra Results (Preliminary) 25
7.2.1 κ Channel 25
7.2.2 $a_0(980)$ Channel 26

8 Conclusions **30**

Chapter 1

Introduction

introduction

Chapter 2

Lattice QCD

QCD = hard

Chapter 3

Building Operators for Finite-Volume Spectroscopy

3.1 Basic Building Blocks

Quarks and gluons are the principle objects of quantum chromodynamics, and form the hadrons which we wish to study. Hence, the operators we use to create hadrons on the lattice are constructed using building blocks of quark and gluon fields. Since hadrons are not point-like objects, but extended composite objects, we form our hadron operators out of *covariantly-displaced* quark fields. In calculating correlator observables on the lattice, two important obstacles must be confronted: noise, and excited-state contamination. With these challenges in mind, our basic building blocks include so-called *stout-smeared* gauge-link field variables and *LapH-smeared* quark field variables. We will see that the stout smearing procedure leads dramatically reduced noise in the evaluation of correlators constructed with displaced operators, and that the LapH-smearing procedure drastically attenuates contributions from higher-lying modes of the theory. Both of these procedures are crucial for extracting the energy spectrum, as we will see in Chapter 5.

3.1.1 Stout Smearing

Ref. [9] describes a smearing procedure for link variables known as stout smearing, which is outlined here. Define $C_\mu(x)$ as the following weighted sum of perpendicular link-variable staples (depicted in Fig. **??**) beginning at a lattice site x and terminating at a neighboring

site $x+\hat{\mu}$,

$$C_\mu(x) = \sum_{\nu\neq\mu} \rho_{\mu\nu} \left(U_\nu(x) U_\mu(x+\hat{\nu}) U_\nu^\dagger(x+\hat{\mu}) \; + U_\nu^\dagger(x-\hat{\nu}) U_\mu(x-\hat{\nu}) U_\nu(x-\hat{\nu}+\hat{\mu}) \right), \quad (3.1)$$

where $\rho_{\mu\nu}$ are tunable real parameters, and $\hat{\mu}$ and $\hat{\nu}$ are unit vectors on the lattice. We use the following weights, which amount to smearing spacial link variables only,

$$\rho_{jk} = \rho, \quad \rho_{4\mu} = \rho_{\mu 4} = 0. \quad (3.2)$$

Next, define a matrix $Q_\mu(x)$ in SU(N) by

$$\begin{aligned} Q_\mu(x) &= \frac{i}{2}\left(\Omega_\mu^\dagger(x) - \Omega_\mu(x)\right) - \frac{i}{2N}\,\mathrm{Tr}\left(\Omega_\mu^\dagger(x) - \Omega_\mu(x)\right) \\ \Omega_\mu(x) &= C_\mu(x) U_\mu^\dagger(x), \qquad \text{(no summation over } \mu). \end{aligned} \quad (3.3)$$

Being both Hermitian and traceless, $Q_\mu(x)$ is also in the Lie algebra $\mathfrak{su}(2)$, and therefore $e^{Q\mu(x)} \in \mathrm{SU}(N)$. Then define an iterative process whereby a link variable at step $n+1$ is related to a link variable at step n as,

$$U_\mu^{(n+1)}(x) = \exp\left(iQ_\mu^{(n)}(x)\right) U_\mu^{(n)}(x). \quad (3.4)$$

Since the link variables we start with are in SU(N) and so is $e^{Q\mu(x)}$, we guarantee that each link variable in this iteration is also in SU(N). This ensures that transforming the link variables in this way preserves the property that they are members of the SU(3) gauge group.

This smearing procedure can be iterated n_ρ times to produce what we refer to as *stout links* and denote by $\tilde{U}_\mu(x)$:

$$U \to U^{(1)} \to U^{(2)} \to \cdots \to U^{(n_\rho)} \equiv \tilde{U}. \quad (3.5)$$

There are two important takeaways of this procedure: only the spatial links are smeared, and all of the symmetries of the original links are preserved.

3.1.2 LapH Smearing

Recall that one can approximate the second derivative of a single-variable function f at a point x as, $f''(x) \approx \frac{f(x+a)+f(x-a)-2f(x)}{2a}$, for small a. Hence, taking a second derivative provides one convention for smearing a function, as it performs a weighted average of the

function in the neighborhood of a point x. On the lattice, we look to the three-dimensional gauge-covariant Laplacian (GCL) to accomplish quark field smearing in a way that preserves the gauge symmetries of the action. In terms of stout smeared link variables, $\tilde{U}_j(x)$, the gauge-covariant Laplacian is defined as,

$$\begin{aligned}\tilde{\Delta}O(x) &= \sum_{k=1}^{3}\left(\tilde{U}_k(x)O(x+\hat{k}) + \tilde{U}_k^\dagger(x-\hat{k})O(x-\hat{k}) - 2O(x)\right),\\ \overline{O}(x)\overleftarrow{\Delta} &= \sum_{k=1}^{3}\left(\overline{O}(x+\hat{k})\tilde{U}_k^\dagger(x) + \overline{O}(x-\hat{k})\tilde{U}_k(x-\hat{k}) - 2\overline{O}(x)\right).\end{aligned} \tag{3.6}$$

Acting the GCL on any operator $O(x)$ preserves all of the single-time-slice symmetry properties of that operator, and therefore so does acting it on that operator any number of times [**?**]. It can be shown [**?**] that when we act the GCL on our quark fields, ψ and $\overline{\psi}$, which are Grassmann-valued, the resultant smeared fields, $\widetilde{\psi}$ and $\widetilde{\overline{\psi}}$, are also Grassmann-valued. One scheme for quark field smearing, defined by [**?**], is,

$$\begin{aligned}\widetilde{\psi}(x) &= \left(1 + \frac{\sigma_s^2}{4n_\sigma}\widetilde{\Delta}\right)^{n_\sigma}\psi(x),\\ \widetilde{\overline{\chi}}(x) &= \overline{\chi}(x)\left(1 + \frac{\sigma_s^2}{4n_\sigma}\overleftarrow{\Delta}\right)^{n_\sigma},\end{aligned} \tag{3.7}$$

where $\sigma_s \in \mathbb{R}$ and $n_\sigma \in \mathbb{Z}$ are tunable parameters.

We can now examine the effect of both link smearing and quark field smearing, using the procedures presented thus far. Fig. 3.1 demonstrates how quark field smearing drastically reduces excited-state contamination in the correlator calculations, and how link smearing drastically reduces signal noise.

$\tilde{\Delta}$ is Hermitian, and we define its eigenvalues as $-\lambda^{(k)}$ (ordered by increasing $\lambda^{(k)}$) and their corresponding orthonormal eigenvectors as $v^{(k)}$. Then, if we define the smearing kernel in Eq. 3.6 as $K = \left(1 + \frac{\sigma_s^2}{4n_\sigma}\widetilde{\Delta}\right)^{n_\sigma}$, we can express the kernel in the eigenbasis of the GCL:

$$K_{ab}(x,y) = \delta_{x_4,y_4}\sum_k w_k\, v_a^{(k)}(x)v_b^{(k)}(y)^*, \tag{3.8}$$

where we suppress the flavor index, and where $w_k \in \mathbb{R}^+$. Since K is written in terms of $\tilde{\Delta}$, it is trivial to write down,

$$w_k = \left(1 - \frac{\sigma_s^2}{4n_\sigma}\lambda^{(k)}\right)^{n_\sigma}. \tag{3.9}$$

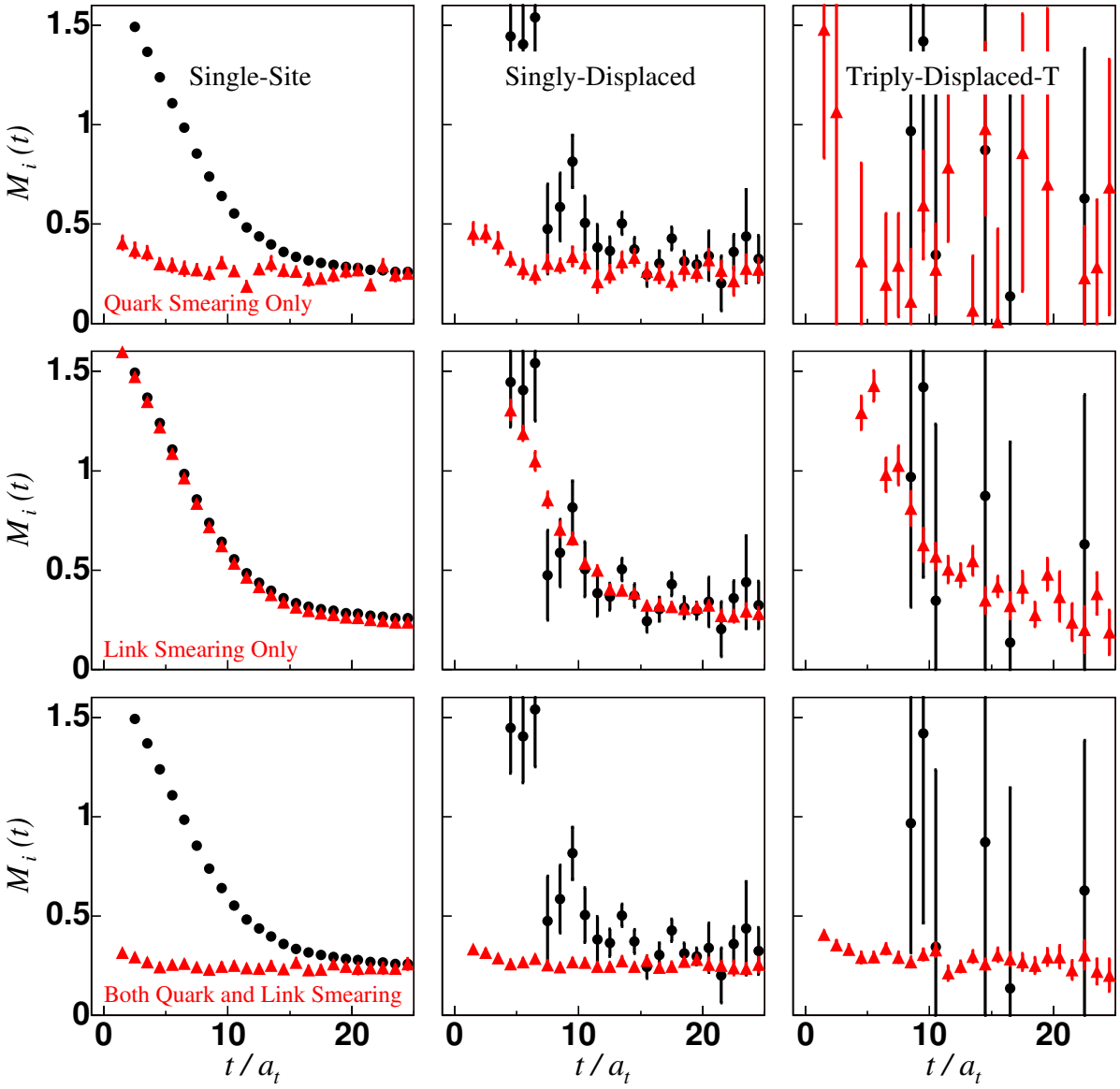

Figure 3.1: Insert caption, cite spectroscopy.

It is then also easy to see that,

$$\lim_{n_\sigma \to \infty} w_k = \exp\left(-\frac{1}{4}\sigma_s^2 \lambda^{(k)}\right). \tag{3.10}$$

We can now see the advantage of working in the eigenbasis of the GCL: the weights, w_k, of higher modes of $\tilde{\Delta}$ are exponentially suppressed. We can then investigate the possibility of modifying the weights to neglect higher-lying contributions. One simple way to accomplish this is the so-called *Laplacian Heaviside* (LapH) smearing scheme, introduced by Peardon, Morningstar, et al. in [10]. This procedure sets the weights to be,

$$w_k = \Theta\left(\sigma_s^2 - \lambda^{(k)}\right), \tag{3.11}$$

where Θ is the Heaviside step function, and σ_s^2 acts as a hard cutoff. The LapH smearing kernel is now defined as

$$\mathcal{S} = \Theta\left(\sigma_s^2 + \widetilde{\Delta}\right), \tag{3.12}$$

and our smeared quark fields are now given by

$$\widetilde{\psi}(x) = \mathcal{S}\psi(x). \tag{3.13}$$

3.1.3 Displacements

The motivation for displacing the quark fields is hadrons are objects which are extended in space. Therefore, if we hope to capture radial and orbital structure when computing the hadronic correlation functions, then we must displace the quark fields, and do so in a gauge-covariant way. The displacements we consider are straight-path displacements along the spatial lattice unit vectors: $j = \pm 1, \pm 2, \pm 3$. We define the gauge-covariant displacement operator in the jth direction by,

$$\widetilde{D}_j^{(p)}(x, x') = \widetilde{U}_j(x)\widetilde{U}_j(x+\hat{j})\ldots\widetilde{U}_j(x+(p-1)\hat{j})\delta_{x',x+p\hat{j}}, \tag{3.14}$$

where $p \geq 1$ denotes the number of steps in by which the field is displaced. For convenience, we also define a zero-displacement operator, $\widetilde{D}_0^{(p)}(x, x') = \delta_{xx'}$. Including color indices a and a', it can be shown that $\widetilde{D}_j^{(p)\dagger}(x, x')^{aa'} = \widetilde{D}_{-j}^{(p)}(x, x')^{aa'}$. From this, the following useful

properties can be derived:

$$\begin{aligned}
\left(\widetilde{D}_j^{(p)}\psi\right)(x) &= \sum_{x'} \widetilde{D}_j^{(p)}(x,x')\,\psi(x') = \widetilde{U}_j(x)\widetilde{U}_j(x+\hat{j})\ldots\widetilde{U}_j(x+(p-1)\hat{j})\psi(x+p\hat{j}),\\
\left(\overline{\chi}\widetilde{D}_j^{(p)\dagger}\right)(x) &= \sum_{x'} \overline{\chi}(x')\,\widetilde{D}_j^{(p)\dagger}(x',x) = \sum_{x'} \overline{\chi}(x')\,\widetilde{D}_{-j}^{(p)}(x',x)\\
&= \overline{\chi}(x+p\hat{j})\widetilde{U}_j^\dagger(x+(p-1)\hat{j})\ldots\widetilde{U}_j^\dagger(x+\hat{j})\widetilde{U}_j^\dagger(x),
\end{aligned} \tag{3.15}$$

from which it can be seen,

$$\overline{\chi}(x)\left(\widetilde{D}_j^{(p)}\psi\right)(x) = \left(\overline{\chi}\widetilde{D}_j^{(p)}\right)(x)\psi(x). \tag{3.16}$$

Why do we have to show associativity? Why would it not be obvious?

The final building blocks for our hadronic operators are *covariantly-displaced, smeared quark fields* and can be summarized as follows:

$$\boxed{\left(\widetilde{D}_{j_1}^{(p)}\ldots\widetilde{D}_{j_n}^{(p)}\widetilde{\psi}\right)_{a\alpha}^{A}, \quad \left(\widetilde{\chi}\widetilde{D}_{j_1}^{(p)\dagger}\ldots\widetilde{D}_{j_n}^{(p)\dagger}\right)_{a\alpha}^{A}, \quad -3 \le j_i \le 3.} \tag{3.17}$$

Add in graphics showing types of displacements we use.

3.2 Symmetries on the Lattice

Symmetries are very useful for characterizing and labeling stationary states in quantum mechanics. Conserved quantities, such as momentum and charge, emerge from the symmetries of a given system, and so in order to identify the relevant quantum numbers of a theory, we must identify its relevant symmetries. The primary symmetries we are interested in are: (cubic) rotations, G-parity, isospin, and flavor. SU(3) gauge symmetry is also vital, but since all of the final objects we study are colorless, it does not contribute to how we label stationary states.

3.2.1 Rotations

Given the nature of a discrete, finite-volume lattice, one can easily see that the SO(3) rotation group is no longer a symmetry group of any lattice gauge theory. Because of this, angular momentum is not conserved on the lattice, and therefore angular momentum is no longer a good quantum number. We will see that instead of using the irreducible representations (irreps) of SO(3) to label stationary states, we use the irreps of the octahedral group.

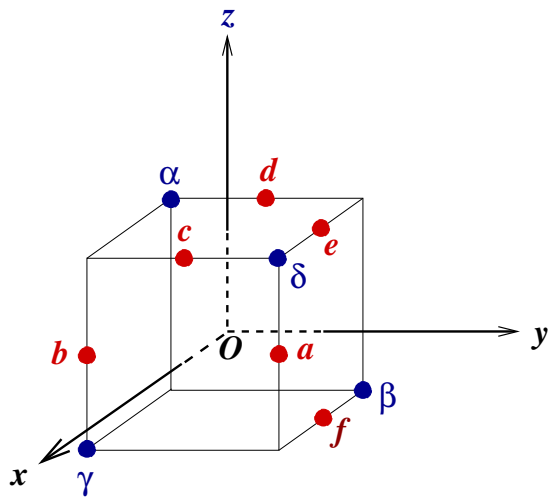

Figure 3.2: The rotation axes corresponding to the rotations C_{nj}. Figure taken from Ref. []

To aid in discussions of cubic rotations on the lattice, the following notation will be used, where the axes of rotation, $j = x, y, z, a, b, c, d, \alpha, \beta, \gamma, \delta$, are shown in Fig. 3.2:

$$\begin{aligned} E &: \text{the identity} \\ C_{nj} &: \text{proper rotation of angle } \frac{2\pi}{n} \text{ about the axis } O_j, \text{ where } n = 2, 3, 4 \\ I_s &: \text{spatial inversion} \end{aligned} \tag{3.18}$$

The octahedral point group, O, consists of all allowed rotations on a three-dimensional spatially-isotropic cubic lattice, and contains the following elements:

Group element	Axes, j
E	
C_{4j}, C_{4j}^{-1}	x, y, z
C_{2j}	$x, y, z, a, b, c, d, e, f$
C_{3j}, C_{3j}^{-1}	$\alpha, \beta, \gamma, \delta$

There are five irreps of O. Following the Mulliken convention [], they are named A_1, A_2, E, T_1, T_2, and they have dimensions 1, 1, 2, 3, 3, respectively. In order to make connections to infinite-volume continuum physics, the Table 3.1 gives the *occurrence numbers* n_Γ^J, which are the number of times the irrep Γ of O occurs in the subduction of the irrep J of SO(3).

When we take the direct product of O with the group $\{E, I_s\}$, thereby adding in spatial inversions to our proper rotations, we get what is known as the point group O_h. This group has twice the number of irreps as O, and so we add the labels g/u (standing for the German *gerade* and *ungerade*) to our irreps, which denote even and odd parity, respectively. The

J	$n^J_{A_1}$	$n^J_{A_2}$	n^J_E	$n^J_{T_1}$	$n^J_{T_2}$
0	1	0	0	0	0
1	0	0	0	1	0
2	0	0	1	0	1
3	0	1	0	1	1
4	1	0	1	1	1
$\vdots$	$\vdots$	$\vdots$	$\vdots$	$\vdots$	$\vdots$

Table 3.1

J	$n^J_{G_1}$	$n^J_{G_2}$	n^J_H
$\frac{1}{2}$	1	0	0
$\frac{3}{2}$	0	0	1
$\frac{5}{2}$	0	1	1
$\frac{7}{2}$	1	1	1
$\frac{9}{2}$	1	0	2
$\vdots$	$\vdots$	$\vdots$	$\vdots$

Table 3.2

irreps of O_h are A_{1g}, A_{1u}, A_{2g}, A_{2u}, E_g, E_u, T_{1g}, T_{1u}, T_{2g}, and T_{2u}.

When we incorporate spin into the picture, we must introduce a new generator that represents rotating by 2π about any axis. Doing so, we arrive at the double octahedral point group O^D. Sparing the group-theoretical details, O^D has three irreps in addition to all of the irreps of O. These are named G_1, G_2, and H, and are of dimension 2, 2, and 4, respectively. Table 3.2 gives the occurrence numbers of these three additional numbers in the subductions of the J irreps of SU(2). Like for O_h, when we incorporate spatial inversions into O^D, we arrive at the double point group O^D_h, which has twice the number of irreps of O^D. The additional irreps are G_{1g}, G_{1u}, G_{2g}, G_{2u}, H_g, and H_u.

Moving irreps

In order to construct operators that create and annihilate particles of definite momentum $\boldsymbol{p}$, we must subduce the representations of O^D_h onto the little group of $\boldsymbol{p}$. The little group of $\boldsymbol{p}$ consists of the subgroup of the abelian group of lattice translations which leave the momentum invariant. For $\boldsymbol{p} = (0,0,0)$, the little group is simply the point group O_h. For any on-axis momentum, e.g. $\boldsymbol{p} = (0,0,1)$, the little group is C_{4v}, which includes four rotations of angle $\frac{\pi}{2}$ about the axis along $\boldsymbol{p}$, as well as four reflections about reflection planes containing that axis. The group elements are contained in three conjugacy classes, which are included in Table 3.3. For any planar-diagonal momentum, e.g. $\boldsymbol{p} = (0,1,1)$, the little group is C_{2v}, the elements and conjugacy classes of which are included in Table 3.4. For any cubic-diagonal fmomentum, e.g. $\boldsymbol{p} = (1,1,1)$, the little group is C_{3v}; its elements and their conjugacy classes are includeds in Table 3.5. Additionally, in order to construct the analogous spinorial little groups (called C^D_{4v}, C^D_{2v}, and C^D_{3v}, respectively), we include the 2π-rotation generator $\overline{E}$. Tables 3.3—3.5 give the elements and conjugacy classes for the spinorial little groups. Finally, the subductions of the irreps of O^D_h onto the above little groups leaves us with the irreps in which we expect to find moving particles. These subductions are given in Table 3.6.

C_{4vD}	
$\mathcal{C}_1$	$\{E\}$
$\mathcal{C}_2$	$\{C_{2z}, \overline{C}_{2z}\}$
$\mathcal{C}_3$	$\{C_{4z}, C_{4z}^{-1}\}$
$\mathcal{C}_4$	$\{I_sC_{2x}, I_sC_{2y}, I_s\overline{C}_{2x}, I_s\overline{C}_{2y}\}$
$\mathcal{C}_5$	$\{I_sC_{2a}, I_sC_{2b}, I_s\overline{C}_{2a}, I_s\overline{C}_{2b}\}$
$\mathcal{C}_6$	$\{\overline{E}\}$
$\mathcal{C}_7$	$\left\{\overline{C}_{4z}, \overline{C}_{4z}^{-1}\right\}$

Table 3.3

C_{2vD}	
$\mathcal{C}_1$	$\{E\}$
$\mathcal{C}_2$	$\{C_{2e}, \overline{C}_{2e}\}$
$\mathcal{C}_3$	$\{I_sC_{2f}, I_s\overline{C}_{2f}\}$
$\mathcal{C}_4$	$\{I_{\overline{c}}C_{2f}, I_s\overline{C}_{2x}\}$
$\mathcal{C}_5$	$\{\overline{E}\}$

Table 3.4

C_{3vD}	
$\mathcal{C}_1$	$\{E\}$
$\mathcal{C}_2$	$\{C_{3\delta}, C_{3\delta}^{-1}\}$
$\mathcal{C}_3$	$\{I_sC_{2b}, I_sC_{2d}, I_sC_{2f}\}$
$\mathcal{C}_4$	$\{\overline{E}\}$
$\mathcal{C}_5$	$\left\{\overline{C}_{3\delta}, \overline{C}_{3\delta}^{-1}\right\}$
$\mathcal{C}_6$	$\{I_s\overline{C}_{2b}, I_s\overline{C}_{2d}, I_s\overline{C}_{2f}\}$

Table 3.5

$\Lambda(O_h)$	$\Lambda(O_h) \downarrow C_{4v}$	$\Lambda(O_h) \downarrow C_{3v}$	$\Lambda(O_h) \downarrow C_{2v}$
A_{1g}	A_1	A_1	A_1
A_{1u}	A_2	A_2	A_2
A_{2g}	B_1	A_2	B_2
A_{2u}	B_2	A_1	B_1
E_g	$A_1 \oplus B_1$	E	$A_1 \oplus B_2$
E_u	$A_2 \oplus B_2$	E	$A_2 \oplus B_1$
T_{1g}	$A_2 \oplus E$	$A_2 \oplus E$	$A_2 \oplus B_1 \oplus B_2$
T_{1u}	$A_1 \oplus E$	$A_1 \oplus E$	$A_1 \oplus B_1 \oplus B_2$
T_{2g}	$B_2 \oplus E$	$A_1 \oplus E$	$A_1 \oplus A_2 \oplus B_1$
T_{2u}	$B_1 \oplus E$	$A_2 \oplus E$	$A_1 \oplus A_2 \oplus B_2$
$G_{1g/u}$	G_1	G	G
$G_{2g/u}$	G_2	G	G
$H_{g/u}$	$G_1 \oplus G_2$	$F_1 \oplus F_2 \oplus G$	$2G$

Table 3.6

3.2.2 Isospin and Quark Flavor

The physical mass of the up quark is $m_u = 2.16^{+0.49}_{-0.26}$ MeV and the physical mass of the down quark is $m_d = 4.67^{+0.48}_{-0.17}$ MeV [12]. While these masses differ by more than a factor of 2, their difference is very small compared to the next heaviest quark, which is the strange quark, measuring at $m_s = 93^{+11}_{-5}$ MeV [12]. Therefore, we find it justfied to make an approximation and set $m_u = m_d$ in our calculations. Since QCD conserves flavor (we do not include electroweak interactions), our theory now possesses an internal SU(2) symmetry, the conserved quantity of which is referred to as *isospin*. This has the same mathematical structure as normal spin, and we can therefore think of it analogously, but it should be stressed that isospin

has no relation to physical space and does not denote any kind of angular momentum. The up quark and down quark states can then be thought of as a doublet of states having total isospin $I = \frac{1}{2}$. Just like with SU(2) spin, isospin can be decomposed onto three axes. By convention, we assign the third isospin axis component of the up quark to be $I_3 = \frac{1}{2}$ and of the down quark to be $I_3 = -\frac{1}{2}$. Their corresponding antiparticles have the same I, but $I_3 \to -I_3$. The work presented here is done in a theory of $N_f = 2 + 1$ QCD, meaning our theory contains two *light* quarks, referring to the up and down quarks (the strange quark is sometimes referred to as a light quark in other contexts), and a strange quark.

Under an SU(2) isospin rotation of the form

$$U_{R_\tau} = \exp\{-i\alpha\tau_3\}\exp\{-i\beta\tau_2\}\exp\{-i\gamma\tau_3\} = \exp(-i\boldsymbol{\varphi}\cdot\boldsymbol{\tau}), \tag{3.19}$$

where τ_1, τ_2, τ_3 are the three generators of isospin rotations, an operator $\overline{O}^{(I)}_{I_3}$ transforms according to the I irreducible representation as

$$U_{R_\tau}\overline{O}^{(I)}_{I_3}U^\dagger_{R_\tau} = \sum_{I'_3}\overline{O}^{(I)}_{I'_3}D^{(I)}_{I'_3,I_3}(R_\tau), \tag{3.20}$$

where $D^{(I)}(R_\tau)$ are the Wigner rotation matrices. In order for an operator $\overline{O}^{(I)}_{I_3}$ to transform irreducibly under isospin, it must satisfy the following properties:

$$\left[\tau_3, \overline{O}^{(I)}_{I_3}\right] = I_3\overline{O}^{(I)}_{I_3}, \tag{3.21}$$

$$\left[\tau_+, \overline{O}^{(I)}_{I_3}\right] = \sqrt{(I-I_3)(I+I_3+1)}\overline{O}^{(I)}_{I_3+1}, \tag{3.22}$$

$$\left[\tau_-, \overline{O}^{(I)}_{I_3}\right] = \sqrt{(I+I_3)(I-I_3+1)}\overline{O}^{(I)}_{I_3-1}, \tag{3.23}$$

$$\left[\tau_3, \left[\tau_3, \overline{O}^{(I)}_{I_3}\right]\right] + \frac{1}{2}\left[\tau_+, \left[\tau_-, \overline{O}^{(I)}_{I_3}\right]\right] + \frac{1}{2}\left[\tau_-, \left[\tau_+, \overline{O}^{(I)}_{I_3}\right]\right] = I(I+1)\overline{O}^{(I)}_{I_3}, \tag{3.24}$$

where $\tau_\pm = \tau_1 \pm i\tau_2$. For annihilation operators, an operator $O^{(I)}_{I_3}$ should transform according to the I irreducible representation as

$$U_{R_\tau}O^{(I)}_{I_3}U^\dagger_{R_\tau} = \sum_{I'_3}O^{(I)}_{I'_3}D^{(I)}_{I'_3,I_3}(R_\tau)^*. \tag{3.25}$$

Annihilation operators that are irreducible under isospin rotations should satisfy:

$$\left[\tau_3, O^{(I)}_{I_3}\right] = -I_3 O^{(I)}_{I_3}, \tag{3.26}$$

$$\left[\tau_+, O^{(I)}_{I_3}\right] = -\sqrt{(I-I_3)(I+I_3+1)}O^{(I)}_{I_3+1}, \tag{3.27}$$

$$\left[\tau_-, O^{(I)}_{I_3}\right] = -\sqrt{(I+I_3)(I-I_3+1)}O^{(I)}_{I_3-1}, \tag{3.28}$$

$$\left[\tau_3, \left[\tau_3, O^{(I)}_{I_3}\right]\right] + \frac{1}{2}\left[\tau_+, \left[\tau_-, O^{(I)}_{I_3}\right]\right] + \frac{1}{2}\left[\tau_-, \left[\tau_+, O^{(I)}_{I_3}\right]\right] = I(I+1)O^{(I)}_{I_3}. \tag{3.29}$$

3.2.3 Charge Conjugation and G-Parity

C-parity can only be a symmetry for electrically neutral states, but as pure QCD does not see electric charge, we are motivated to generalize C-parity in order to account states in a charged isospin multiplet, such as the pion triplet. With $\mathcal{C}$ denoting the charge conjugation operator, G-parity can be explicitly defined as

$$U_G = \mathcal{C}e^{-i\pi\tau_2}. \tag{3.30}$$

Since charge conjugation is a symmetry of the strong interaction, then when isospin is also a symmetry, G-parity must be a symmetry as well. The basic building blocks transform under G-parity as follows [**?**]:

$$U_G\left(D_j\mathcal{S}\psi(x)\right)^u_{a\alpha} U_G^\dagger = -\left(\chi\mathcal{S}D_j^\dagger(x)\right)^d_{a\beta}\Gamma^G_{\beta\alpha}, \tag{3.31}$$

$$U_G\left(D_j\mathcal{S}\psi(x)\right)^d_{a\alpha} U_G^\dagger = \left(\chi\mathcal{S}D_j^\dagger(x)\right)^u_{a\beta}\Gamma^G_{\beta\alpha}, \tag{3.32}$$

$$U_G\left(D_j\mathcal{S}\psi(x)\right)^s_{a\alpha} U_G^\dagger = -\left(\chi\mathcal{S}D_j^\dagger(x)\right)^s_{a\beta}\Gamma^G_{\beta\alpha}, \tag{3.33}$$

$$U_G\left(\chi\mathcal{S}D_j^\dagger(x)\right)^u_{a\alpha} U_G^\dagger = -\Gamma^C_{\alpha\beta}\left(D_j\mathcal{S}\psi(x)\right)^u_{a\beta}, \tag{3.34}$$

$$U_G\left(\chi\mathcal{S}D_j^\dagger(x)\right)^a_{a\alpha} U_G^\dagger = \Gamma^G_{\alpha\beta}\left(D_j\mathcal{S}\psi(x)\right)^u_{a\beta'}, \tag{3.35}$$

$$U_G\left(\chi\mathcal{S}D_j^\dagger(x)\right)^s_{a\alpha} U_G^\dagger = -\Gamma^C_{\alpha\beta}\left(D_j\mathcal{S}\psi(x)\right)^s_{a\beta}. \tag{3.36}$$

3.2.4 Projecting Operators onto Symmetry Sectors

3.3 Single-Hadron Operator Construction

3.3.1 Baryon Operators

Baryon states are classified according to: momentum $\boldsymbol{p}$, total spin J, spin projection J_z (or any other axis), parity P (± 1), and quark flavor. The flavor quantum numbers we consider are isospin I and its projection I_3, and strangeness S. We require that baryon operators are also gauge-invariant. As a reminder, the basic building blocks for the baryon operators are covariantly-displaced smeared quark fields.

A simple *elemental* operator that creates a baryon at a definite position with appropriate color and flavor structure is denoted by $B_i^F(\boldsymbol{x}, t)$

3.3.2 Meson Operators

3.3.3 Tetraquark Operators

3.4 Multi-Hadron Operator Construction

Chapter 4

Monte Carlo Calculation of Correlators

Chapter 5

Correlator Analysis: Determining the Finite-Volume Spectrum

Chapter 6

Scattering Resonances in a Two-Scalar Field Theory

ϕ/ρ

Chapter 7

Investigating the Tetraquark Content of the Light Scalar Mesons κ and $a_0(980)$

In this chapter, we examine the effect of including tetraquark operators on the spectrum in the scalar meson sectors containing the $K_0^*(700)$ (here and often elsewhere referred to as the κ) and the $a_0(980)$ in $N_f = 2 + 1$ QCD, using an anisotropic lattice with gauge field configurations generated by the Hadron Spectrum Collaboration []. It has been suggested that the κ and $a_0(980)$ could have tetraquark content [6, 3, 4, 7], and to date, there have been a small number of studies investigating tetraquarks on the lattice using light quarks. In 2010, Prelovsek et al. investigated the σ and κ as possible tetraquark candidates, but neglected disconnected diagrams in their calculations [11]. Using tetraquark interpolators, they found an additional light state in both the σ and κ channels. In 2013, the ETM collaboration examined the $a_0(980)$ and κ using four-quark operators [2], though they also neglected disconnected diagrams in their calculations. They found no evidence of an additional state that can be interpreted as a tetraquark. In 2018, Alexandrou et al. conducted a study of the $a_0(980)$ with four-quark operators [1], including disconnected contributions. In their study, they found an additional finite-volume state in the sector containing the $a_0(980)$ meson, which couples to a diquark-antidiquark interpolating field, in the range of ... to ... Additionally, they conclude that disconnected diagrams have drastic effects on their results, and thus cannot be neglected.

We perform Monte Carlo calculations using 412 gauge field configurations on an anisotropic ($\frac{a_s}{a_t} \approx 3.451$) lattice of size $32^3 \times 256$, with a length of 3.74 fm and a pion mass of approximately 230 MeV. We extract two spectra in each symmetry channel: one using a basis of only single- and two-meson operators, and one using a basis that also includes a tetraquark

operator selected from hundreds of tetraquark operators which were tested. We find that including a tetraquark operator yields an additional finite-volume state in each symmetry channel: one rangeing from ... to ... in the κ channel, and one ranging from ... to ... in the $a_0(980)$ channel. In this work, we use the stochastic LapH method [8] to evaluate all diagrams in our calculations, including *all* disconnected contributions.

7.1 Operator construction

We include single- and two- meson operators, as well as tetraquark operators, in the basis of interpolating operators. We construct our elemental operators using building blocks of smeared, gauge-covariantly displaced quark fields, and stout-smeared link variables. To form the final operators out of our elemental operators, we project the elemental operators onto various symmetry channels according to isospin, parity, G-parity, octahedral little group, etc. That is, to form a meson operator $M_l(t)$ that transforms irreducibly under all symmetries of interest (labeled by the compound index l) at time t, we must take a linear combination of our elemental meson operators, $M_l(t) = c^{(l)}_{\alpha\beta}\Phi^{AB}_{\alpha\beta}(\boldsymbol{p}, t)$. To form a two-meson operator $\mathcal{O}_l(t)$, we would follow a similar procedure and project the product of two final meson operators $M^a_{l_a}(t)M^b_{l_a}(t)$ onto a final symmetry channel l: $\mathcal{O}_l(t) = c^{(l)}_{l_a l_b} M^a_{l_a}(t)M^b_{l_a}(t)$.

In order to construct a tetraquark operator, we must consider the various ways to construct a color-singlet four-quark object out of four quark fields. As seen in Ref. [5], the Clebsch-Gordon decompositions show that the only way to construct a color-singlet is by using two quarks and two antiquarks, and that doing so yields two linearly independent color singlet objects:

$$\begin{aligned}
3 \otimes 3 \otimes 3 \otimes 3 &= 3 \oplus 3 \oplus 3 \oplus \overline{6} \oplus \overline{6} \oplus 15 \oplus 15 \oplus 15 \oplus 15, \\
3 \otimes 3 \otimes 3 \otimes \overline{3} &= \overline{3} \oplus \overline{3} \oplus \overline{3} \oplus 6 \oplus 6 \oplus 6 \oplus \overline{15} \oplus \overline{15} \oplus 24, \\
3 \otimes 3 \otimes \overline{3} \otimes \overline{3} &= 1 \oplus 1 \oplus 8 \oplus 8 \oplus 8 \oplus 8 \oplus 10 \oplus \overline{10} \oplus 27.
\end{aligned} \tag{7.1}$$

There are 81 basis vectors formed by the quark fields, $p^*_a(x)q^*_b(x)r_c(x)s_d(x)$, where each r, s transforms as a color vector in the fundamental 3 irrep, and so, p^*, q^* transform in the $\overline{3}$ irrep. We need two linearly independent and gauge-invariant combinations of these to exhaust all possible tetraquark operators. It is easy to see that the following combinations are both linearly independent and gauge-invariant (and thus form our elemental tetraquark operators):

$$\begin{aligned}
T_S &= (\delta_{ac}\delta_{bd} + \delta_{ad}\delta_{bc})\, p^*_a(x)q^*_b(x)r_c(x)s_d(x) \\
T_A &= (\delta_{\alpha c}\delta_{bd} - \delta_{\alpha d}\delta_{bc})\, p^*_\alpha(x)q^*_b(x)r_c(x)s_d(x).
\end{aligned} \tag{7.2}$$

These elemental tetraquark operators are combinations of two gauge-invariant quark-antiquark constituents. The individual constituents are *not* mesons since they separately do not have well-defined quantum numbers. In other words, we project the entire elemental tetraquark operator onto relevant symmetry channels, rather than each individual quark-antiquark operator.

While we chose only a handful of tetraquark operators for our final analysis, we designed hundreds of operators with differing flavor structures and displacements. We tested these operators by individually adding them to a basis of single- and multi-meson operators to see if an additional level was found. Most of the operators did not yield an additional level, but we found particular operators that did. In the κ channel, we tested the following flavor structures: $\bar{s}u\bar{s}s$, $\bar{s}u\bar{u}u$, $\bar{s}u\bar{d}u$. We found that only operators with the $\bar{s}u\bar{s}s$ flavor structure yielded an additional finite-volume state. We tested both single-site and quadruple displacements, and found operators of both types that yielded additional finite-volume states. The quadruply-displaced operators came at a higher computational cost and offered no improvements, and so were excluded from the final operator sets. In the $a_0(980)$ channel, we tested the following flavor structures: $\bar{u}u\bar{d}u$, $\bar{s}s\bar{d}u$, $\bar{d}u\bar{d}u$. We found that only operators with the $\bar{u}u\bar{d}u$ flavor structure yielded an additional finite-volume state. We only tested single-site operators in the $a_0(980)$ channel, after finding no improvement with other displacement types in the κ channel. We also constructed operator bases that included several tetraquark operators, and found that the number of additional levels in the energy range we examined was unchanged.

7.2 Lattice Spectra Results (Preliminary)

7.2.1 κ Channel

We summarize results obtained by fitting a spectrum in the κ at-rest symmetry channel for two operator bases: one including only single-meson and two-meson operators, and one including single-meson, two-meson, and tetraquark operators. Figure 7.1 shows the spectrum with and without the inclusion of a tetraquark operator in the basis. The tetraquark operator is of the flavor structure $\bar{s}u\bar{s}s$, is of the antisymmetric form in Eq. (7.2), and has no quark displacement. We found that single-site ($\boldsymbol{d_\alpha} = \boldsymbol{d_\beta} = 0$) tetraquark operators resulted in better (less noisy) correlator signals than displaced operators. We see that including a tetraquark operator yields an additional finite-volume state in the range of $(2.178-2.256)m_K$, which is not present when only single- and two-meson operators are used. Additionally, a plot of the overlap factors for the tetraquark operator (Figure **??**) shows significant overlap

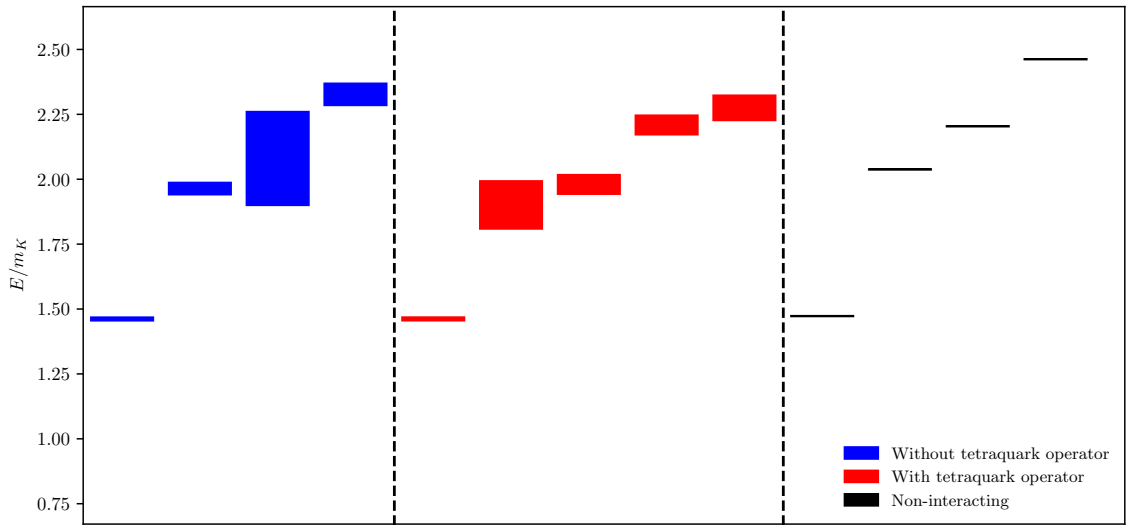

Figure 7.1: The first five and six levels of the spectrum in the κ at-rest symmetry channel. On the left: the spectrum obtained using a basis with no tetraquark operators. In the middle: the spectrum obtained using one tetraquark operator. On the right: non-interacting levels shown for reference, where $(\boldsymbol{d}^2)$ denotes particles with squared momentum $(2\pi\boldsymbol{d}/L)^2$.

onto this extra state (level 3 in the plot). This suggests that there is a finite-volume state in our lattice spectrum that shares quantum numbers with the κ resonance, and that has tetraquark content. Whether or not this is evidence of the κ resonance having tetraquark content, however, will have to wait for future scattering studies using Lüscher's method.

7.2.2 $a_0(980)$ Channel

We summarize results obtained by fitting a spectrum in the $a_0(980)$ at-rest symmetry channel for again for two operator bases as in the κ channel. Figure 7.3 shows the spectrum with and without the inclusion of a tetraquark operator in the basis. The tetraquark operator is of the flavor structure $\overline{u}u\overline{d}u$, is also of the antisymmetric form in (7.2), and again has no quark displacement. We again found that using single-site tetraquark operators resulted in better correlator signals than displaced operators. We see an extra level appear in the range of $(2.258 - 2.426)m_K$ when we include a tetraquark operator. Again, overlap factors are shown for the tetraquark operator, and significant overlaps with the additional level (level 3) can be seen in Figure **??**. This suggests there is a finite-volume state in our lattice spectrum that shares quantum numbers with the $a_0(980)$ resonance, and that has tetraquark content.

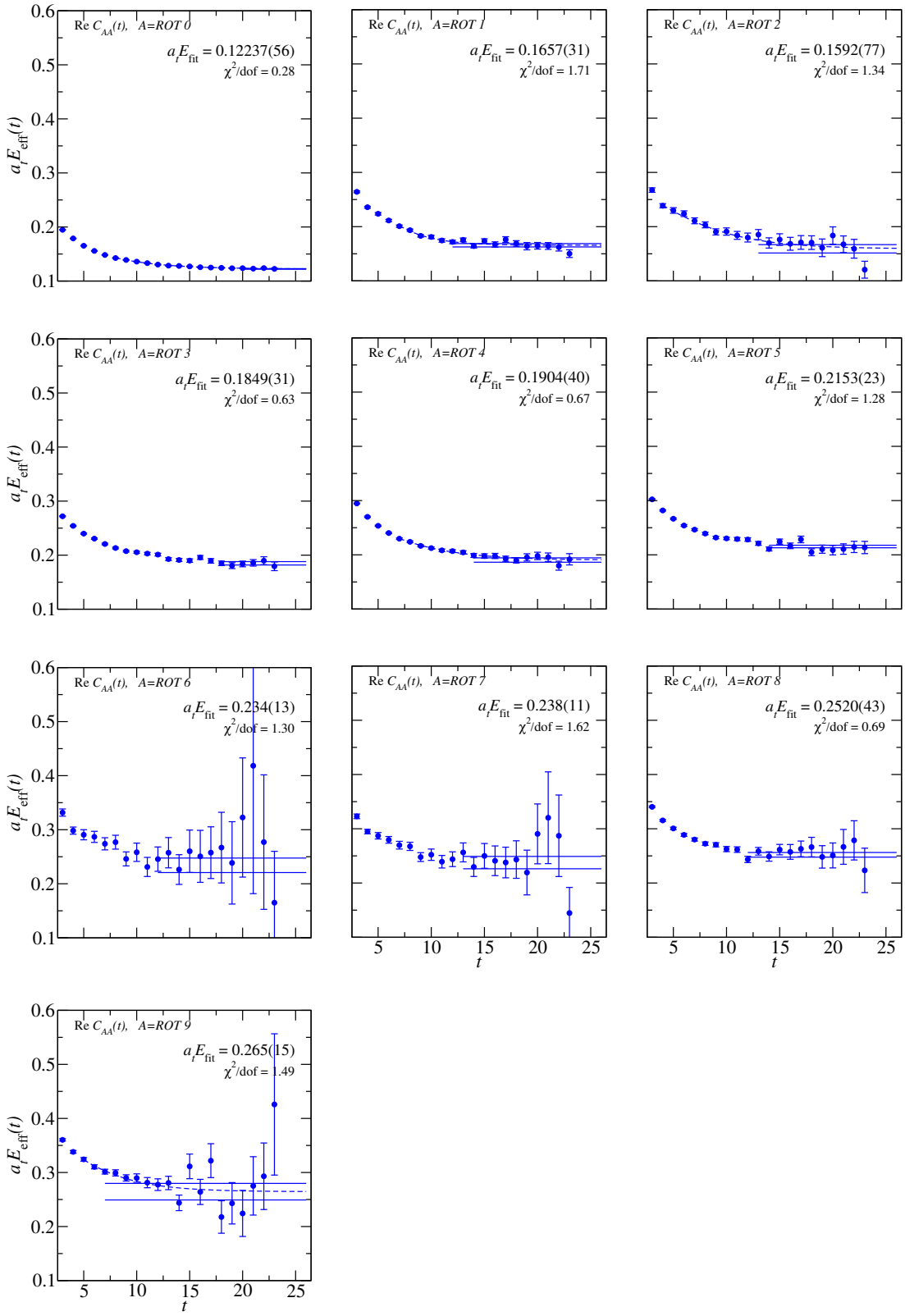

Figure 7.2: Effective energies for the rotated 10x10 correlator matrix in the κ channel. Effective energy curves calculated from correlator fits are overlaid, and fit results are shown.

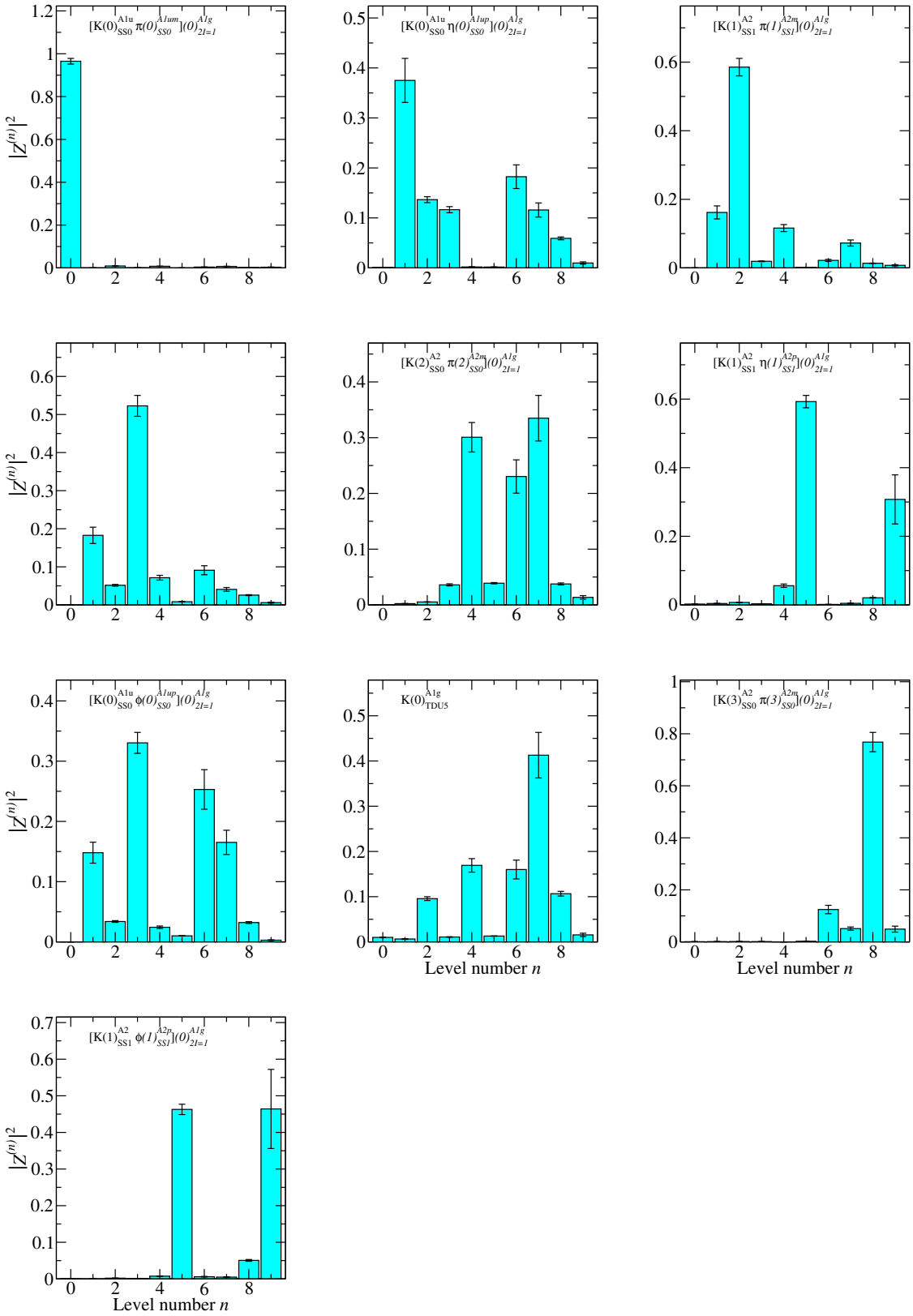
$[K(0)^{A1u}_{SS0}\,\pi(0)^{A1um}_{SS0}](0)^{A1g}_{2I=1}$
$[K(0)^{A1u}_{SS0}\,\eta(0)^{A1up}_{SS0}](0)^{A1g}_{2I=1}$
$[K(1)^{A2}_{SS1}\,\pi(1)^{A2m}_{SS1}](0)^{A1g}_{2I=1}$
$[K(2)^{A2}_{SS0}\,\pi(2)^{A2m}_{SS0}](0)^{A1g}_{2I=1}$
$[K(1)^{A2}_{SS1}\,\eta(1)^{A2p}_{SS1}](0)^{A1g}_{2I=1}$
$[K(0)^{A1u}_{SS0}\,\phi(0)^{A1up}_{SS0}](0)^{A1g}_{2I=1}$
$K(0)^{A1g}_{TDU5}$
$[K(3)^{A2}_{SS0}\,\pi(3)^{A2m}_{SS0}](0)^{A1g}_{2I=1}$
$[K(1)^{A2}_{SS1}\,\phi(1)^{A2p}_{SS1}](0)^{A1g}_{2I=1}$
$|Z^{(n)}|^2$
Level number n

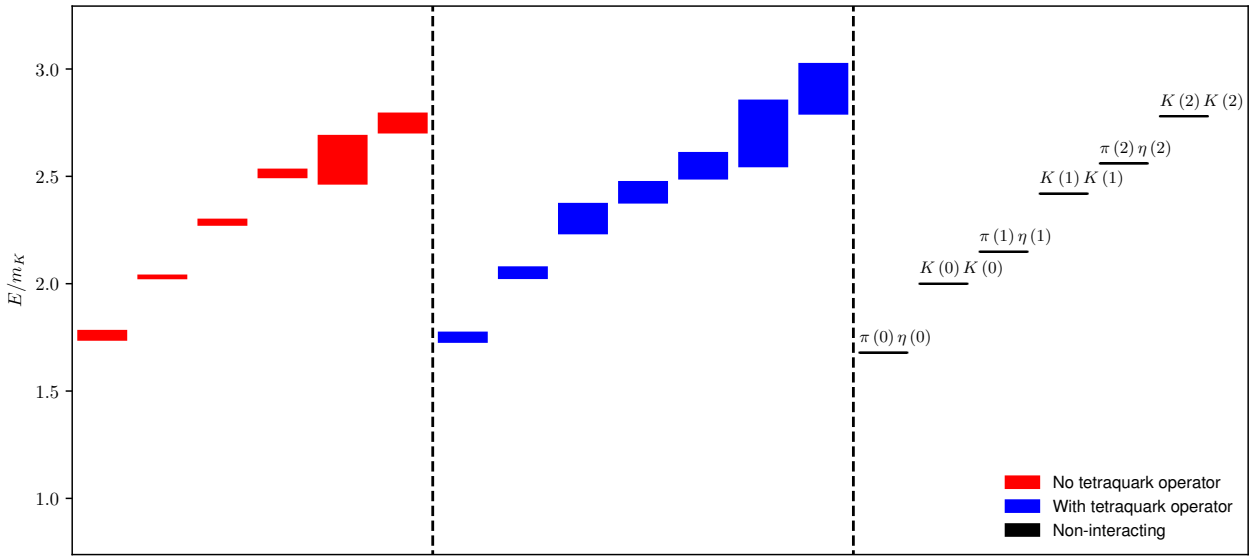

Figure 7.3: The first six and seven levels of the spectrum in the $a_0(980)$ at-rest symmetry channel. On the left: the spectrum obtained using a basis with no tetraquark operators. In the middle: the spectrum obtained using one tetraquark operator. On the right: non-interacting levels shown for reference, where $(\boldsymbol{d}^2)$ denotes particles with squared momentum $(2\pi\boldsymbol{d}/L)^2$.

As in the κ-channel case, evidence for or against the $a_0(980)$ having tetraquark content will have to wait for future scattering studies done by applying Lüscher's method.

Chapter 8

Conclusions

Bibliography

[1] Constantia Alexandrou, Joshua Berlin, Mattia Dalla Brida, Jacob Finkenrath, Theodoros Leontiou, and Marc Wagner. Lattice QCD investigation of the structure of the $a_0(980)$ meson. *Physical Review D*, 97, 2018.

[2] Constantia Alexandrou, Jan Oliver Daldrop, Mattia Dalla Brida, Mario Gravina, Luigi Scorzato, Carsten Urbach, and Marc Wagner. Lattice investigation of the scalar mesons $a_0(980)$ and κ using four-quark operators. *JHEP04*, page 137, 2013.

[3] Claude Amsler and Nils A. Törnqvist. Mesons beyond the naive quark model. *Physics Reports*, 389(2):61 – 117, 2004.

[4] Frank E. Close and Nils A. Törnqvist. Scalar mesons above and below 1 GeV. *Journal of Physics G: Nuclear and Particle Physics*, 28(10):R249–R267, aug 2002.

[5] Andrew D. Hanlon. The ρ meson spectrum and kπ scattering with partial wave mixing in lattice QCD. January 2018.

[6] R. L. Jaffe. Exotica. *Phys. Rept.*, 409:1–45, 2005. [,191(2004)].

[7] L. Maiani, F. Piccinini, A. D. Polosa, and V. Riquer. New look at scalar mesons. *Phys. Rev. Lett.*, 93:212002, Nov 2004.

[8] Colin Morningstar, John Bulava, Justin Foley, Keisuke J. Juge, David Lenkner, Mike Peardon, and Chik Him Wong. Improved stochastic estimation of quark propagation with Laplacian Heaviside smearing in lattice QCD. *Phys. Rev.*, D83:114505, 2011.

[9] Colin Morningstar and Mike Peardon. Analytic smearing of SU(3) link variables in lattice QCD. *Phys. Rev. D*, 69:054501, Mar 2004.

[10] Michael Peardon, John Bulava, Justin Foley, Colin Morningstar, Jozef Dudek, Robert G. Edwards, Bálint Joó, Huey-Wen Lin, David G. Richards, and Keisuke Jimmy Juge. Novel quark-field creation operator construction for hadronic physics in lattice qcd. *Phys. Rev. D*, 80:054506, Sep 2009.

[11] Sasa Prelovsek, Terrence Draper, Christian B. Lang, Markus Limmer, Keh-Fei Liu, Nilmani Mathur, and Daniel Mohler. Lattice study of light scalar tetraquarks with $I = 0, 2, \frac{1}{2}, \frac{3}{2}$: Are σ and κ tetraquarks? *Physical Review D*, 82(9):094507, nov 2010.

[12] M. Tanabashi, K. Hagiwara, K. Hikasa, K. Nakamura, Y. Sumino, F. Takahashi, J. Tanaka, K. Agashe, G. Aielli, C. Amsler, M. Antonelli, D. M. Asner, H. Baer, Sw. Banerjee, R. M. Barnett, T. Basaglia, C. W. Bauer, J. J. Beatty, V. I. Belousov, J. Beringer, S. Bethke, A. Bettini, H. Bichsel, O. Biebel, K. M. Black, E. Blucher, O. Buchmuller, V. Burkert, M. A. Bychkov, R. N. Cahn, M. Carena, A. Ceccucci, A. Cerri, D. Chakraborty, M.-C. Chen, R. S. Chivukula, G. Cowan, O. Dahl, G. D'Ambrosio, T. Damour, D. de Florian, A. de Gouvêa, T. DeGrand, P. de Jong, G. Dissertori, B. A. Dobrescu, M. D'Onofrio, M. Doser, M. Drees, H. K. Dreiner, D. A. Dwyer, P. Eerola, S. Eidelman, J. Ellis, J. Erler, V. V. Ezhela, W. Fetscher, B. D. Fields, R. Firestone, B. Foster, A. Freitas, H. Gallagher, L. Garren, H.-J. Gerber, G. Gerbier, T. Gershon, Y. Gershtein, T. Gherghetta, A. A. Godizov, M. Goodman, C. Grab, A. V. Gritsan, C. Grojean, D. E. Groom, M. Grünewald, A. Gurtu, T. Gutsche, H. E. Haber, C. Hanhart, S. Hashimoto, Y. Hayato, K. G. Hayes, A. Hebecker, S. Heinemeyer, B. Heltsley, J. J. Hernández-Rey, J. Hisano, A. Höcker, J. Holder, A. Holtkamp, T. Hyodo, K. D. Irwin, K. F. Johnson, M. Kado, M. Karliner, U. F. Katz, S. R. Klein, E. Klempt, R. V. Kowalewski, F. Krauss, M. Kreps, B. Krusche, Yu. V. Kuyanov, Y. Kwon, O. Lahav, J. Laiho, J. Lesgourgues, A. Liddle, Z. Ligeti, C.-J. Lin, C. Lippmann, T. M. Liss, L. Littenberg, K. S. Lugovsky, S. B. Lugovsky, A. Lusiani, Y. Makida, F. Maltoni, T. Mannel, A. V. Manohar, W. J. Marciano, A. D. Martin, A. Masoni, J. Matthews, U.-G. Meißner, D. Milstead, R. E. Mitchell, K. Mönig, P. Molaro, F. Moortgat, M. Moskovic, H. Murayama, M. Narain, P. Nason, S. Navas, M. Neubert, P. Nevski, Y. Nir, K. A. Olive, S. Pagan Griso, J. Parsons, C. Patrignani, J. A. Peacock, M. Pennington, S. T. Petcov, V. A. Petrov, E. Pianori, A. Piepke, A. Pomarol, A. Quadt, J. Rademacker, G. Raffelt, B. N. Ratcliff, P. Richardson, A. Ringwald, S. Roesler, S. Rolli, A. Romaniouk, L. J. Rosenberg, J. L. Rosner, G. Rybka, R. A. Ryutin, C. T. Sachrajda, Y. Sakai, G. P. Salam, S. Sarkar, F. Sauli, O. Schneider, K. Scholberg, A. J. Schwartz, D. Scott, V. Sharma, S. R. Sharpe, T. Shutt, M. Silari, T. Sjöstrand, P. Skands, T. Skwarnicki, J. G. Smith, G. F. Smoot, S. Spanier, H. Spieler, C. Spiering, A. Stahl, S. L. Stone, T. Sumiyoshi, M. J. Syphers, K. Terashi, J. Terning, U. Thoma, R. S. Thorne, L. Tiator, M. Titov, N. P. Tkachenko, N. A. Törnqvist, D. R. Tovey, G. Valencia, R. Van de Water, N. Varelas, G. Venanzoni, L. Verde, M. G. Vincter, P. Vogel, A. Vogt, S. P. Wakely, W. Walkowiak, C. W. Walter, D. Wands, D. R. Ward, M. O. Wascko, G. Weiglein, D. H. Weinberg, E. J. Weinberg, M. White, L. R.

Wiencke, S. Willocq, C. G. Wohl, J. Womersley, C. L. Woody, R. L. Workman, W.-M. Yao, G. P. Zeller, O. V. Zenin, R.-Y. Zhu, S.-L. Zhu, F. Zimmermann, P. A. Zyla, J. Anderson, L. Fuller, V. S. Lugovsky, and P. Schaffner. Review of particle physics. *Phys. Rev. D*, 98:030001, Aug 2018.